

GCN-DevLSTM: Path Development for Skeleton-Based Action Recognition

Lei Jiang¹, Weixin Yang^{2,4}, Xin Zhang³ and Hao Ni^{1,4}

¹ University College London, London, UK

² University of Oxford, Oxford, UK

³ South China University of Technology, Guangzhou, Guangdong, China

⁴ The Alan Turing Institute, London, UK

lei.j@ucl.ac.uk, weixin.yang@maths.ox.ac.uk, eexinzhang@scut.edu.cn, h.ni@ucl.ac.uk

Abstract

Skeleton-based action recognition (SAR) in videos is an important but challenging task in computer vision. The recent state-of-the-art (SOTA) models for SAR are primarily based on graph convolutional neural networks (GCNs), which are powerful in extracting the spatial information of skeleton data. However, it is yet clear that such GCN-based models can effectively capture the temporal dynamics of human action sequences. To this end, we propose the G-Dev layer, which exploits the path development – a principled and parsimonious representation for sequential data by leveraging the Lie group structure. By integrating the G-Dev layer, the hybrid G-DevLSTM module enhances the traditional LSTM to reduce the time dimension while retaining high-frequency information. It can be conveniently applied to any temporal graph data, complementing existing advanced GCN-based models. Our empirical studies on the NTU60, NTU120 and Chalearn2013 datasets demonstrate that our proposed GCN-DevLSTM network consistently improves the strong GCN baseline models and achieves SOTA results with superior robustness in SAR tasks. The code is available at <https://github.com/DeepIntoStreams/GCN-DevLSTM>.

1 Introduction

Action recognition has a wide range of applications in diverse fields such as human-computer interaction, performance assessment in athletics, virtual reality, and video monitoring [Liu *et al.*, 2019a]. In comparison to video-based action recognition, skeleton-based action recognition (SAR) exhibits better robustness to the variety of light conditions and its efficiency in computation and storage [Chen *et al.*, 2021; Shi *et al.*, 2019] while preserving data privacy. Skeleton data can be obtained either by localization of 2D/3D human joints using the depth camera [Liu *et al.*, 2019a] or pose estimation algorithms from the videos [Cao *et al.*, 2017].

Despite extensive literature devoted to SAR, the challenge still remains open. The key step towards accurate SAR

models lies in designing an effective spatio-temporal representation of the skeleton sequence. Previously, Recurrent Neural Networks (RNNs) were commonly used due to their strength in capturing temporal dynamics. The advent of Spatial Temporal Graph Convolutional Networks (STGCN) has shifted the focus towards Graph Convolutional Networks (GCNs), which incorporate both spatial graph convolution and temporal convolution. The majority of subsequent GCN-based approaches [Chen *et al.*, 2021; Shi *et al.*, 2020; Cheng *et al.*, 2020b; Cheng *et al.*, 2020a; Song *et al.*, 2020; Zhou *et al.*, 2022], following the STGCN framework, focus on the improvement of the spatial graph convolution, with minimal emphasis on improving temporal modules. These methods utilize 1-D temporal convolution operation to capture temporal features. However, whether convolution operation is most effective for capturing temporal dynamics is in question.

On the other hand, Rough path theory [Lyons, 1998] originated as a branch of stochastic analysis to make sense of controlled differential equations driven by highly oscillatory paths. More recently, the applications of rough path theory in sequential data analysis are emerging. In particular, the path signature, as a fundamental object of Rough path theory, has successful applications in various domains ranging from finance to healthcare, demonstrating its capacity as a principled and efficient feature of time series. By embedding time series into the continuous path space, the signature offers a unified treatment to handle variable length and irregular sampling. Signature-based algorithms show promise across diverse fields, including SAR task [Liao *et al.*, 2021; Yang *et al.*, 2022; Ahmad *et al.*, 2019; Li *et al.*, 2019a; Cheng *et al.*, 2023]. However, the path signature may face challenges such as the curse of dimensionality caused by high path dimension and lack of adaptability due to its deterministic nature [Lou *et al.*, 2022]. To address these, Lou *et al.* [Lou *et al.*, 2022] propose the path development from rough path theory, as a trainable alternative to path signature. The path development enjoys the desirable properties of the signature while reducing feature dimension significantly. [Lou *et al.*, 2022] shows that combining the path development under the appropriate Lie group with LSTM [Hochreiter and Schmidhuber, 1997] alleviates the gradient vanishing of LSTMs, leading to significant enhancement across various sequential tasks.

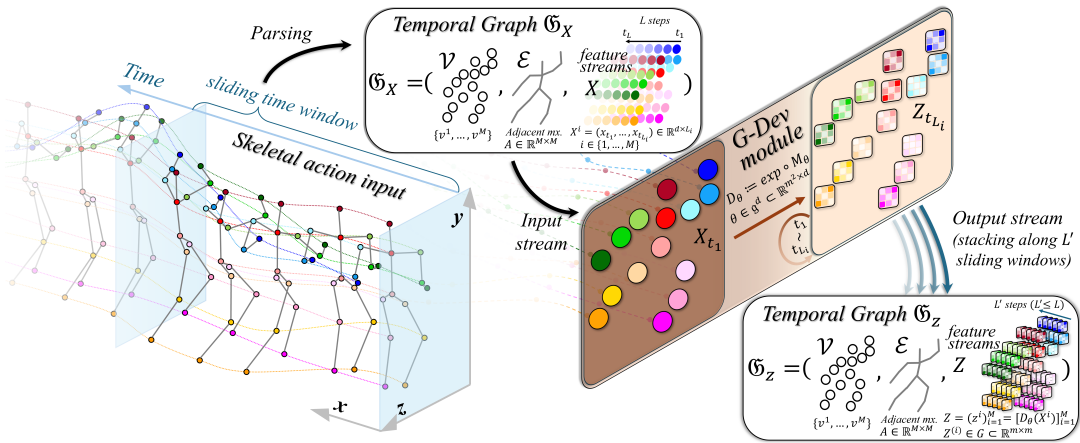


Figure 1: The work flow of G-Dev layer.

This paper places a primary emphasis on enhancing the temporal module within our framework. To this end, we introduce a novel G-Dev layer (as shown in Figure 1) on the temporal graph, which refers to the graph with the node feature as time series. This layer utilizes the sliding window to summarize the local information via the principled path development, offering time dimension benefit and robustness to missing data and irregular sampling. Moreover, we propose the GCN-DevLSTM network, composed of the CNN-based branch and G-Development-based branch for SAR. While retaining the effectiveness of graph convolution for modeling spatial relationships among joints, the GCN-DevLSTM network exploits the hybrid capacity of G-Dev layer and LSTM for handling temporal dynamics. Our GCN-DevLSTM is flexible to incorporate with different GCN backbones. This combination captures discriminative temporal features and improves performance. Experimental results on three commonly used datasets Chalearn 2013, NTU 60 and NTU 120 show that our approach with the GCN backbone being topology-non-shared graph from CTRGCN [Chen *et al.*, 2021] outperforms other methods, demonstrating the effectiveness and robustness of our proposed temporal module.

We summarize our main contributions as follows:

- We design a novel and principled graph development (**G-Dev**) layer for analyzing temporal graph data by extending the path development originally applied to vector-valued time series. As a generic network on graph data with time-varying node attributes, G-Dev exhibits efficacy and robustness to irregular sampling and missing data.
- We introduce the novel **GCN-DevLSTM** network for skeleton-based action recognition that effectively combines the G-Dev layer with LSTM to capture complex temporal dynamics.
- Experimental results demonstrate that our designed model outperforms other state-of-the-art models in SAR in terms of *accuracy* and *robustness*.

2 Related Work

2.1 Skeleton-based Action Recognition

The main challenge in SAR is extracting the effective representation that captures both spatial and temporal dependency of skeleton sequences. Earlier methods typically use convolutional neural networks (CNNs) [Chéron *et al.*, 2015; Liu *et al.*, 2017b] and RNN [Du *et al.*, 2015; Liu *et al.*, 2017a] to address this challenge without considering structural topology. STGCN [Yan *et al.*, 2018] is the first method to capture spatial and temporal relationships using GCN, taking the skeleton topology of the graph into consideration while this topology is not learnable, with only the spatial connection between adjacent joints being connected. As a result, some actions that rely on non-adjacent joints may lead to poor results. [Liu *et al.*, 2020] tackles this issue by introducing a learnable adjacency matrix alongside the original manually defined one, enabling connections between non-neighboring joints. Yet, this approach maintains the same graph for all action inputs, which might not be ideal, as different action classes may benefit from different graph topologies. To address this, [Li *et al.*, 2019b; Shi *et al.*, 2019; Shi *et al.*, 2020] propose adaptive GCN with the learnable and data-driven topology that shares among all channels. [Cheng *et al.*, 2020a; Chen *et al.*, 2021] further propose the non-shared topology for each channel. Current GCN-based methods mainly focus on the enhancement of the graph representation, with limited attention to temporal design. In particular, most GCN-based methods typically use CNNs to capture temporal dynamics. Although studies such as [Si *et al.*, 2019; Zhao *et al.*, 2019; Liao *et al.*, 2021] attempt to incorporate LSTM with GCN for the SAR tasks, these methods still significantly underperform the sota GCN models that combine both GCN and CNN on large-scale action datasets.

2.2 Path signature & Path Development

The path signature is a core object of rough path theory, which provides a rigorous way of making sense of the solution to controlled differential equations driven by rough signals [Lyons *et al.*, 2007; Lyons, 1998]. Playing a role as the

non-commutative monomials on the path space, the path signature can be used as a faithful feature of time series [Lyons, 2014; Levin *et al.*, 2013], which leads to applications for various sequential data learning tasks, such as handwritten recognition [Xie *et al.*, 2017], writer identification [Yang *et al.*, 2015], financial data analysis [Lyons *et al.*, 2014], time-series data generation [Ni *et al.*, 2021] and SAR [Liao *et al.*, 2021; Cheng *et al.*, 2023; Yang *et al.*, 2022; Ahmad *et al.*, 2019; Li *et al.*, 2019a]. In the specific context of SAR, [Ahmad *et al.*, 2019] focuses on employing path signature solely for extracting spatial features while [Yang *et al.*, 2022; Li *et al.*, 2019a] utilize path signature to obtain both temporal and spatial features. However, relying solely on path signature to capture spatial relationships may be suboptimal, as it is not data adaptive and only considers local spatial correlations. [Liao *et al.*, 2021] leverages GCN to extract spatial features and employ the log signature to capture temporal dynamics. However, the network tends to overfit rapidly when increasing its depth due to the curse of dimensionality of the signature for the high dimensional path.

More recently, the path development layer [Lou *et al.*, 2022] is proposed as a general sequential layer on time series data as a trainable alternative to the signature feature. It has useful applications in supervised learning on sequential data [Lou *et al.*, 2022] and synthetic time generation [?]. This layer is inspired by the (Cantani) development of a path [Driver, 1995]. The path development serves as a useful mathematical tool in rough path theory for proving the properties of the path signature (see e.g., [Hambly and Lyons, 2010; Chevyrev and Lyons, 2016]). In particular, [Chevyrev and Lyons, 2016] proves that under an appropriate Lie group, the path development is a universal and characteristic feature of the path signature, which provides the theoretical support for the development layer [Lou *et al.*, 2022]. Building upon [Lou *et al.*, 2022], our work extends the application of the path development from the vector-valued time series to that of the temporal graph.

3 G-Dev Layer: Development layer of a temporal graph

In this section, we start with a concise overview of the development of the path as the principled feature representation of d -dimensional time series. Subsequently, we proceed with introducing the path development layer proposed in [Lou *et al.*, 2022]. For details of the path development, we refer readers to [Lou *et al.*, 2022]. Building on this, we propose the G-Dev layer, a novel extension of the development layer applied to temporal graphs, wherein the features of nodes are represented by time series.

3.1 The development of a Path

Let $X \in V([0, T], \mathbb{R}^d)$, where $V([0, T], \mathbb{R}^d)$ represents the space of continuous paths of finite length in \mathbb{R}^d defined on the time interval $[0, T]$. To fix the notations, let G denote a finite-dimensional Lie group and its associate Lie algebra \mathfrak{g} . Examples of the matrix Lie algebra associated with the special orthogonal group (denoted by \mathfrak{so}) and special Euclidean

group (\mathfrak{se}) are given as follows:

$$\begin{aligned} \mathfrak{gl}(m; \mathbb{F}) &= \{m \times m \text{ matrices over } \mathbb{F}\} \cong \mathbb{F}^{m \times m} \quad (\mathbb{F} = \mathbb{R} \text{ or } \mathbb{C}) \\ \mathfrak{so}(m, \mathbb{R}) &:= \{A \in \mathfrak{gl}(m; \mathbb{R}) : A^T + A = 0\} \\ \mathfrak{se}(m) &= \left\{ \begin{bmatrix} \omega & v \\ 0 & 0 \end{bmatrix} \mid \omega \in \mathfrak{so}(m, \mathbb{R}), v \in \mathbb{R}^m \right\} \end{aligned}$$

Definition 3.1 (Path Development). Let $M : \mathbb{R}^d \rightarrow \mathfrak{g} \subset \mathfrak{gl}(m)$ be a linear map. The path development of $X \in V([0, T], \mathbb{R}^d)$ on G under M is the solution $Z_T \in G$ to the below equation

$$dZ_t = Z_t \cdot M(dX_t) \quad \text{for all } t \in [0, T] \quad \text{with } Z_0 = \text{Id}_m, \quad (1)$$

where Id_m is the identity matrix and \cdot denotes the matrix multiplication.

Example 1 (Linear path). Let $X \in V([0, T], \mathbb{R}^d)$ be a linear path. For any linear map $M \in L(\mathbb{R}^d, \mathfrak{g})$, the development of the path under M admits the explicit formula and is simply

$$D_M(X)_{0,T} = \exp(M(X_T - X_0)), \quad (2)$$

where \exp is the matrix exponential.

Thanks to the multiplicative property of the path development (Lemma 2.4 in [Lou *et al.*, 2022]), the development of two paths $X \in V([0, s], \mathbb{R}^d)$ and $Y \in V([s, t], \mathbb{R}^d)$ under M is the same as the development of the concatenation of these two paths, in formula,

$$D_M(X * Y) = D_M(X) \cdot D_M(Y), \quad (3)$$

where $X * Y$ denotes the concatenation of X and Y and \cdot is the matrix multiplication. Eq. (3) enables us to compute the development of any piecewise linear path explicitly.

The path development enjoys several desirable theoretical properties, making it a principled and efficient representation of sequential data. We summarize the following two properties, that are directly relevant to action recognition.

Invariance under Time-reparametrization Similar to the path signature, the path development is invariant under time reparametrization. This property ensures that the development of a path remains unchanged irrespective of the speed at which the path is traversed. It is well suited to action recognition, as the prediction of actions should not depend on the speed of the actions or the frame rate. Time-reparametrization invariance of path development may bring massive dimension reduction and enhance the robustness to variation in speed.

Uniqueness of the path development Intuitively, the path development effectively captures the order of events in time series, leveraging the non-commutative nature of matrix multiplication. Changing the order of events may lead to different development in general, highlighting its capacity to capture the temporal dynamics of sequential data. It is proven in [Chevyrev and Lyons, 2016] the path development is a characteristic and universal feature of an un-parameterized path in $V_1([0, T], \mathbb{R}^d)$ under the appropriate Lie group. In other words, transforming a path of finite length to its development map $M \mapsto \text{Dev}_M(X)$ can uniquely determine the path X up to translation. Thus, the path development combined with the starting point effectively summarizes the path without any loss of information.

3.2 Path Development Layer

Proposed in [Lou *et al.*, 2022], the path development layer is a novel neural network inspired by the path development by exploiting the representation of the matrix Lie group. More specifically, this layer utilizes the parameterized linear map $M \in L(\mathbb{R}^d, \mathfrak{g})$ by its linear coefficients $\theta \in \mathfrak{g}^d$.

Definition 3.2 (Path development layer). The path development layer, denoted by D_θ , is defined as a mapping $\mathbb{R}^{d \times (N+1)} \rightarrow G$, which transforms any input time series $x = (x_1, x_2, \dots, x_N)$ to the development $z_N \in G$ under the trainable linear map $M_\theta \in L(\mathbb{R}^d, \mathfrak{g})$. For $n \in \{0, \dots, N-1\}$, we set

$$z_{n+1} = z_n \exp(M_\theta(x_{n+1} - x_n)), z_0 = Id_m, \quad (4)$$

where $\theta \in \mathfrak{g}^d$ is the model parameter.

Eq. (4) is a direct consequence of Example 1 and the multiplicative property of the development (Eq. (3)). Moreover, Eq. (4) shows the recurrence as an analogy to that of the RNNs, albeit in a much simpler manner, as depicted in Figure 1 (lower panel). Similar to RNNs, the path development can cope with time series input of variable length.

Dimension reduction The output of the path development has dimension m^2 , where m is the matrix size. Note that its dimension does not depend on the path dimension d and time dimension T , resulting in the massive dimension reduction. This is in stark contrast to the signature feature of degree k , whose dimension $\left(\sum_{i=0}^k d^i = \frac{d^{k+1}-1}{d-1}\right)$ grows geometrically w.r.t d . Moreover, the path development is well suited to extract information from high-frequency time series or long time series without concern on the curse of dimensionality.

Robustness to irregular sampling As the path development can be interpreted as a solution to the differential equation (Eq. (1)), it is a continuous time series model. Similar to other continuous time models such as signature and Neural CDEs [Kidger *et al.*, 2020], the path development exhibits robustness in handling time series data with irregular sampling.

Computational Efficiency of analyzing online data Multiplicative property of the path development allows incremental computation of the development layer in streaming data, thereby reducing both computational load and memory requirements.

3.3 G-Dev Layer: Apply path development layer to a temporal graph

In this subsection, we propose the so-called G-Dev Sequence Layer, which extracts the local information of the temporal graph using the development layer in a rolling window fashion. The core component of the G-Dev Sequence layer serves as a generalization of the development layer from the d -dimensional time series to the temporal graph.

Throughout this paper, the temporal graph $\mathfrak{G}_X = (\mathcal{V}, \mathcal{E}, X)$ refers to the graph with each node associated with d -dimensional time series features X . Here $\mathcal{V} := \{v^1, \dots, v^M\}$ denotes the vertex set and \mathcal{E} can be represented by the adjacent matrix $A \in \mathbb{R}^{M \times M}$. We consider the general case where the time dimension of each node may vary across the nodes. More specifically, Let $X^i = (x_{t_1}, \dots, x_{t_{L_i}}) \in$

$\mathbb{R}^{d \times L_i}$ denote the features of the i^{th} vertex, where d and N_i are the path and time dimension, respectively. The feature sets $X = (X^{(1)}, \dots, X^{(M)})$ is obtained by stacking X^i for all $i \in \{1, \dots, M\}$. Clearly, the skeleton sequence is an example of temporal graph data.

G-Dev module. Let us first define the G-Dev module, which is a trainable layer with model parameters $\theta \in \mathfrak{g}^d \subset \mathbb{R}^{m^2 \times d}$, where m is the matrix order of development. It maps a temporal graph $\mathfrak{G}_X = (\mathcal{V}, \mathcal{E}, X)$ to a static graph with matrix-valued features $\mathfrak{G}_Z = (\mathcal{V}, \mathcal{E}, Z)$ by applying the path development to the time-augmented transformation of each feature vector X_i of the vertex v_i , as shown in Figure 1. In formula, for each vertex index $i \in \{1, \dots, M\}$, the output feature is $Z = (Z^{(i)})_{i=1}^M$, where $Z^{(i)} = D_\theta(X^{(i)}) \in G \subset \mathbb{R}^{m \times m}$.

Built on top of the G-Dev module, we employ a sliding window strategy to construct the following G-Dev Sequence layer, which can summarize (potentially long) time series over coarse time partitions to reduce the time dimension effectively while retaining the fine-grained information by using the low-dimensional representation.

Without loss of generality, let us focus on the case where the graph features X share the same time stamps $(t_i)_{i=0}^{L-1}$ across vertices¹. Fix the window (kernel) size K and stride S . Let $L' = \lceil \frac{L-K}{S} \rceil$. By applying padding to Y , for any $Y \in \mathbb{R}^{d \times N}$, we define a sequence of time series \tilde{Y}_j :

$$\tilde{Y}_j = (Y_{j \times S}, \dots, Y_{j \times S + K - 1}) \in \mathbb{R}^{d \times K}, \forall j \in \{0, \dots, L' - 1\}. \quad (5)$$

Definition 3.3 (G-Dev Sequence layer). A G-Dev (Sequence) layer with the matrix degree m , window size K and stride S is defined as a trainable map that takes a temporal graph $\mathfrak{G}_X = (\mathcal{V}, \mathcal{E}, X)$ with $X \in \mathbb{R}^{M \times L' \times d}$ as an input and outputs a temporal graph $\mathfrak{G}_Z = (\mathcal{V}, \mathcal{E}, Z)$ with model parameter $\theta \in \mathbb{R}^{d \times m \times m}$. Here $Z = (z_j)_{j=1}^{L'}$ is a time series consisting of $z_j \in \mathbb{R}^{m \times m \times m}$. Each $z_j = \text{G-Dev}_\theta(\tilde{X}_j)$, where \tilde{X}_j is obtained by applying sliding window by Eqn. 5.

The G-Dev Sequence layer (Definition 3.3) can be easily extended to the moving window with the dilation parameter D , where we collect the path information at every D time steps during each moving window. To guarantee no information loss of the G-Dev sequence layer, it is crucial to choose S and K to ensure a minimum one-point overlap between two consecutive moving windows.

4 GCN-DevLSTM Network for SAR

A skeleton sequence can be modeled by a temporal graph, where the vertex set corresponds to M possible joints, with each $v^i \in \mathbb{R}^2$ or \mathbb{R}^3 indicating 2 or 3D coordinates of the i^{th} joint, respectively. The edge set \mathcal{E} denotes the set of all the joint pairs connected by a bone.

In Figure 2(a), we introduce the proposed GCN-DevLSTM Network, a novel framework for SAR tasks that integrates the GCN and DevLSTM modules into a single block. The GCN

¹Otherwise, we apply linear interpolation for data imputation, which would not affect the development feature thanks to invariance to time re-parameterization.

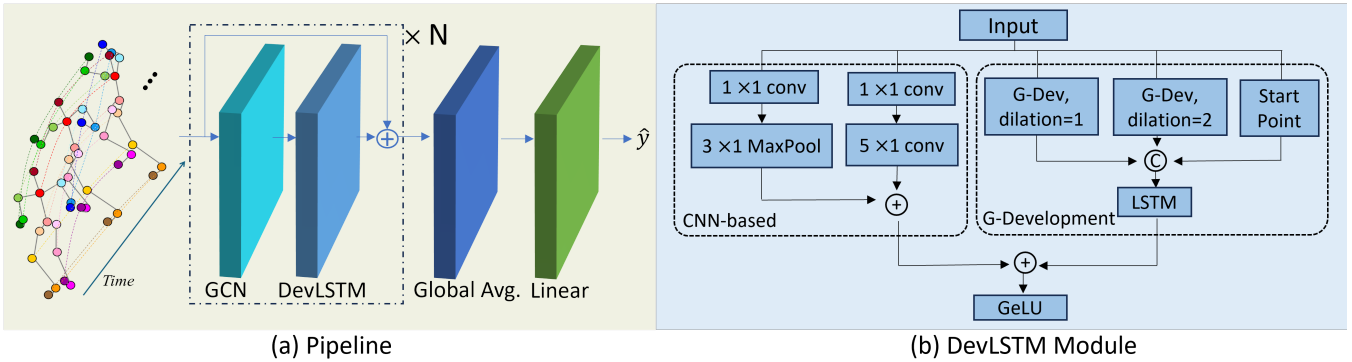


Figure 2: (a) The pipeline of our proposed approach consists of N blocks, with each block containing a GCN module and a DevLSTM module. (b) The detail of the DevLSTM module.

module is designed to detect spatial correlations among vertices, while the DevLSTM module handles the temporal dynamics across video frames. Further details on these modules are discussed in Sections 4.1 and 4.2, respectively. Our network is designed to capture discriminative spatial-temporal features with N such blocks, where $N = 9$ in this paper. Additionally, within each block, we build a residual path that establishes a shortcut connection with the input to mitigate gradient vanishing/ explosion issues, enhancing the training stability.

Following these GCN-DevLSTM blocks, we employ global average pooling to effectively reduce both temporal and spatial dimensions to 1. After that, a linear function is applied to adjust the feature dimension to match the number of action classes, thereby facilitating the classification process. Cross-entropy loss is employed at the end to compare the predicted action class with the ground truth.

4.1 GCN Module

In the GCN module, we basically follow the network of CTR-GC [Chen *et al.*, 2021]. However, we depart from the use of three initial adjacency matrices representing self, inward, and outward correlations. Instead, we propose a Hops-CTRGC to enhance the model by incorporating various hops of information to construct three adjacency matrices denoted as A_0 , A_1 , and A_2 .

A_0 remains an identical (self) matrix. For A_1 , the elements a_{ij} are set to 1 if vertex i and vertex j are physically connected in the skeleton graph; otherwise, a_{ij} in A_1 is set to 0. A_1 captures the direct connections in the graph. To enrich spatial information, we introduce $A_2 = A_1^2$, enabling a vertex to connect with its neighbour’s neighbour. A_2 allows us to extend our understanding beyond direct connections to include relationships involving two hops in the graph. Since GCN module is not our main focus in this paper, readers can find more details about the network of CTR-GC in [Chen *et al.*, 2021] or in our supplementary material 7.5.

4.2 G-DevLSTM Module

The proposed DevLSTM module, illustrated in Figure 2(b) is mainly composed of the CNN-based branch and the G-development-based branch. The output of DevLSTM module

is given by applying GeLU activation function to the summation of the output of both branches.

G-Development branch. Inspired by the design of multi-scale TCN [Liu *et al.*, 2020], we also design a multi-scale network to capture temporal dynamics. We utilize two G-dev layers with the dilation parameter $D = 1$ and $D = 2$ to enhance its ability to capture temporal patterns across different scales in the input sequence.

The path development combined with the starting point can determine the path uniquely. Hence, we append the location of the starting points to the output of the path development layer along the feature dimension over each sub-time interval. The resulting features are then fed into an LSTM network, which is able to effectively aggregate the local development summary and learn deep features to extract the long-term dependencies in time series data. We use the sequential output of LSTM, which keeps the time dimension the same as the input.

CNN-based branch. MaxPool and a convolutional layer with 5×1 kernel size have consistently demonstrated superior performance within the temporal module of other GCN-based studies. Introducing both MaxPool and the 5×1 convolutional operation to our DevLSTM temporal module has the potential to enhance model performance even further. We can reasonably design kernel size, padding, stride and dilation to ensure the output size of Maxpool, LSTM and 5×1 convolution remain the same.

5 Numerical Experiments

To validate the effectiveness of the proposed approach, we carry out numerical experiments on the following popular benchmarking datasets for skeleton-based action and gesture recognition. These datasets are chosen for their diversity in data size and task complexity, providing a comprehensive evaluation of the model’s performance. (1) **Chalearn2013** [Escalera *et al.*, 2013] is a public dataset for gesture recognition, consisting of 11,116 skeleton examples and 20 gesture categories, filmed by 27 people. Each frame has 20 joints. (2) **NTU RGB+D 60** (NTU-60) [Shahroudy *et al.*, 2016] consists of 56,880 action samples and 60 action classes, filmed by 40 people using three Kinect cameras in

Table 1: Experimental results on NTU-60 and NTU-120 dataset. The best results for each benchmark are bolded.

	Venue	NTU-60		NTU-120						
		X-sub (%)	X-view (%)	X-sub (%)	X-view (%)					
ST-GCN [Yan <i>et al.</i> , 2018]	AAAI'18	81.5	88.3	70.7	73.2					
AGC-LSTM [Si <i>et al.</i> , 2019]	ICCV'19	89.2	95.0	-	-					
Bayesian-LSTM [Zhao <i>et al.</i> , 2019]	ICCV'19	81.8	89.0	-	-					
2S-AGCN [Shi <i>et al.</i> , 2019]	CVPR'19	88.5	95.1	82.5	84.2					
MS-AAGCN [Shi <i>et al.</i> , 2020]	TIP'20	90.0	96.2	-	-					
Shift-GCN [Cheng <i>et al.</i> , 2020b]	CVPR'20	90.7	96.5	85.9	87.6					
Logsig-RNN [Liao <i>et al.</i> , 2021]	BMVC'21	-	-	75.8	78.0					
CTR-GCN(J) [Chen <i>et al.</i> , 2021]	ICCV'21	89.8	94.8	84.9	86.7					
CTR-GCN(J+B) [Chen <i>et al.</i> , 2021]	ICCV'21	92.0	96.3	88.7	90.1					
CTR-GCN [Chen <i>et al.</i> , 2021]	ICCV'21	92.4	96.8	88.9	90.6					
EfficientGCN [Song <i>et al.</i> , 2022]	TPAMI'22	92.1	96.1	88.7	88.9					
Ta-CNN [Xu <i>et al.</i> , 2022]	AAAI'22	90.4	94.8	85.4	86.8					
FR-Head [Zhou <i>et al.</i> , 2023]	CVPR'23	92.8	96.8	89.5	90.9					
Our methods	Joint	✓				90.8	95.7	86.2	87.7	
	Bone		✓			91.1	95.2	87.0	88.6	
	Dual			✓		91.2	95.3	87.1	88.7	
	Joint motion				✓	92.4	96.4	89.0	90.4	
	Bone motion					✓	92.6	96.6	89.3	90.7
			✓			✓	92.9	96.6	89.7	91.2

different camera views. 3D skeletal data in the dataset have different sequence lengths, with each owning 25 joints. (3) **NTU RGB+D 120** (NTU-120) [Liu *et al.*, 2019b] extends upon NTU RGB+D 60, consisting of 114,480 samples and 120 action classes, filmed by 106 people in three camera views. We consider the Cross-subject (X-Sub) and Cross-view (X-View) evaluation benchmarks for both NTU-60 and NTU-120 as proposed by Shahroudy *et al.* (2016). We use only skeleton data from these datasets for our experiments.

Experiments are conducted using a single Nvidia A6000 graphics card, where a batch of 16 examples is fed to the network. Stochastic gradient descent optimiser [Bottou, 2012] is employed, with a Nesterov momentum = 0.9 and a weight decay = 0.0003. The training epoch is set to 65 and we apply the warm-up strategy [He *et al.*, 2016] to the first 5 epochs. The initial learning rate is 0.02 and a step learning rate decay is applied with a factor of 0.1 at epoch 35 and 55, respectively. Data processing on NTU datasets mainly follows the procedure in [Chen *et al.*, 2021], with the length of all input data sequences resizing to 64. We use \mathfrak{se} Lie algebra in this paper, with a corresponding matrix size of $m = 10$. A detailed network architecture can be found in the supplementary. The replicate padding is used in our experiments.

5.1 Fusion results from different data streams

Most of the recent approaches that we are set to compare combine predicted scores from different input data streams for enhanced performance. The most commonly used data streams are joint (J), bone (B), joint motion (JM) and bone motion (BM) where details can be found in [Shi *et al.*, 2019; Shi *et al.*, 2020]. Apart from the above-mentioned data streams, we introduce a novel stream: the dual graph (D). In a dual graph, vertices represent bones, and edges establish connections between these bones. More details about dual graph can be found at Supplementary 7.1.

5.2 Comparison with state-of-the-art methods

We compare our approach with other state-of-the-art methods on both NTU-60 and NTU-120 datasets, as shown in Table 1. Since our GCN module is following CTR-GCN [Chen *et al.*, 2021] with the major difference lying in the temporal module, we show more results on CTR-GCN for a more comprehensive comparison. As we can see all of our results, no matter whether using only joint or using ensembled streams combining joint and bone, outperform CTR-GCN with a large margin on all benchmarks. Our method's limited performance gain with extra joint or bone motion, compared to CTR-GCN, may stem from our path development layer exploiting position differences between consecutive time points. As a result, streams using joint and bone motion provide identical information at the beginning of the network, limiting their help. Our model, integrating five data streams, achieves the best result compared to other state-of-the-art approaches across three out of four benchmarks.

Table 2 shows the comparison results between our result and other state-of-the-art methods on Chalearn2013 dataset. We only employ the joint stream for fair comparison as other approaches only use the joint representation on Chalearn2013 dataset. It is evident that our model yields the best result on the small-scale gesture dataset, proving its effectiveness on the small dataset. It is important to highlight that our network

Table 2: Results on Chalearn2013 dataset.

	Acc (%)
ST-LSTM + Trust Gate [Liu <i>et al.</i> , 2018]	92.00
Multi-path CNN [Liao <i>et al.</i> , 2019]	93.13
3s_net_TTM [Li <i>et al.</i> , 2019a]	92.08
GCN-Logsig-RNN [Liao <i>et al.</i> , 2021]	92.86
CTR-GCN [Chen <i>et al.</i> , 2021]	95.19
ST-PSM+L-PSM [Cheng <i>et al.</i> , 2023]	94.18
Our method	95.61

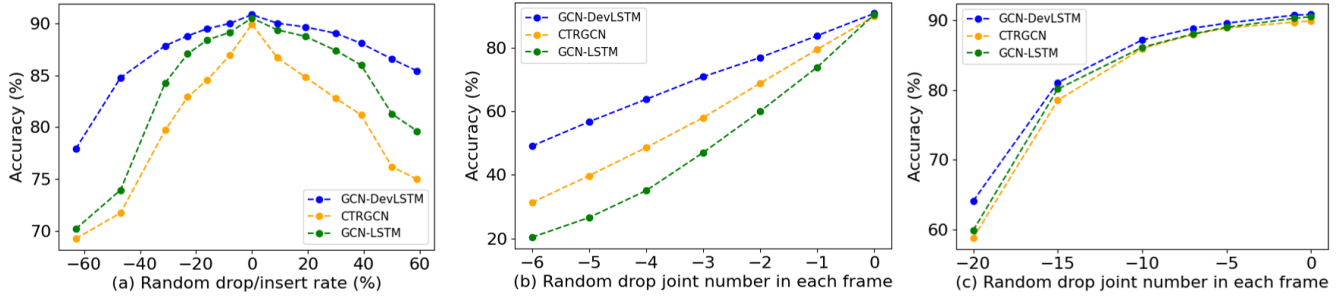


Figure 3: Robustness analysis on NTU60 X-sub benchmark.

Table 3: Comparison between our DevLSTM module with MS-TCN across various GCN modules on NTU60 dataset.

CTR-GC	MS-TCN (J)	90.3	94.9
	DevLSTM (J)	90.8	95.7
AGC	MS-TCN (J)	89.8	94.5
	DevLSTM (J)	90.6	95.6
Fixed graph	MS-TCN (J)	88.7	93.1
	DevLSTM (J)	89.5	94.5

structure remains the same on all datasets, demonstrating its strong adaptability for different dataset sizes.

5.3 Comparison with signature-based models

Compared to the Logsig-RNN [Liao *et al.*, 2021], one of the recent signature-based action recognition methods (using the joint stream only), our model (J) outperforms 10.4% and 9.7% respectively on both benchmarks of NTU-120 dataset, and 2.75% on Chalearn2013 dataset. Compared to the latest signature-based action recognition approach [Cheng *et al.*, 2023], we still outperform 1.43% on Chalearn2013 dataset while unfortunately, they didn’t report their results on NTU dataset, leaving no way to compare. These results support the advantages of using path development that we claimed before, compared with path signature.

5.4 Comparison with MS-TCN

To demonstrate the flexible integration of our DevLSTM temporal module with various GCN modules in a plug-and-play fashion, we employ the adaptive graph convolution (AGC) graph in 2S-AGCN [Shi *et al.*, 2019] and a fixed graph without learnable parameters, respectively as an additional GCN module backbone in our network. In addition, we compare our DevLSTM with multi-scale temporal convolution network (MS-TCN) used in [Chen *et al.*, 2021] across the different GCN backbones. Table 3 illustrates that the proposed DevLSTM module consistently outperforms MS-TCN with different GCN backbones by a large margin, indicating that our designed temporal module is effective in enhancing various GCN backbones. An overview of adaptive graph convolution and fixed graph can be found in the supplementary material.

Table 4: Ablation studies of DevLSTM module on NTU-60 dataset. w/o means without.

Components	X-sub	X-view
with all components (J)	90.8	95.7
w/o residual path (J)	89.9	95.2
w/o 1×1 conv & 5×1 conv (J)	90.7	95.3
w/o 1×1 conv & 3×1 maxpool (J)	90.6	95.4
w/o path dev (J)	90.5	95.2

5.5 Ablation studies

We further investigate the importance of residual path design to connect the input and output of each block and each component in our temporal module. As evident from Table 4, residual path plays an important role to enhance the model performance since it can help alleviate gradient vanishing/explosion in the deep neural network. For temporal components in our DevLSTM module, the path development layer emerges as the primary contributor to the overall performance improvement since removing it causes the largest performance degradation, with other components also contributing to enhanced performance.

5.6 Robustness Analysis

We comprehensively compare the robustness of our full model (GCN-DevLSTM), CTRGCN [Chen *et al.*, 2021] and our model without path development layer (GCN-LSTM) in terms of missing frames, missing joints and variable sequence length. To this end, we firstly create a new test dataset by randomly dropping or inserting a certain number of frames out of 64 frames to test the robustness of missing frames and variable length. Figure 3a illustrates that our full model with the path development layer consistently outperforms the other methods in terms of accuracy, regardless of the proportion of frames missing or inserting, proving its robustness to irregular sampling and variable sequence length.

Additionally, to validate the robustness of missing joints due to occlusions in real life, we create another dataset by randomly dropping a certain number of joints in each frame. To fill in these missing joints, two techniques are adopted: zero-filling (in Figure 3b) and linear interpolation (in Figure 3c). Both figures show that our model with G-Dev layer, is consistently more robust against missing joints than others. More details are in the supplementary material.

6 Conclusion and future work

Conclusion. In summary, we propose a novel and general **GCN-DevLSTM** network for analyzing temporal graph data by leveraging the path development layer. This approach not only offers flexibility when combined with various GCN modules but also significantly enhances performance by effectively capturing the temporal dependencies within data. The effectiveness of the proposed method is validated by the state-of-the-art results on both small gesture data and large action datasets in SAR. Moreover, it demonstrates superior robustness to missing data and variable frame rates. **Limitation.** The current G-Dev Sequence layer relies on other GCNs to extract spatial information, which limits its standalone utility. Future enhancements could include integrating the features of adjacent nodes directly into the input of the path development layer to better capture spatio-temporal dependencies. **Broader impact** Our proposed G-Dev Sequence layer provides a generic model for temporal graph data, opening up possibilities for its applications across various fields, including urban planning, social network analysis and others.

Acknowledgements. LJ, WY and HN are supported by the EPSRC [grant number EP/S026347/1]. WY and HN are also supported by The Alan Turing Institute under the EPSRC grant EP/N510129/1.

References

- [Ahmad *et al.*, 2019] Tasweer Ahmad, Lianwen Jin, Jialuo Feng, and Guozhi Tang. Human action recognition in unconstrained trimmed videos using residual attention network and joints path signature. *IEEE Access*, 7:121212–121222, 2019.
- [Bottou, 2012] Léon Bottou. Stochastic gradient descent tricks. In *Neural Networks: Tricks of the Trade: Second Edition*, pages 421–436. Springer, 2012.
- [Cao *et al.*, 2017] Zhe Cao, Tomas Simon, Shih-En Wei, and Yaser Sheikh. Realtime multi-person 2d pose estimation using part affinity fields. In *IEEE Conference on Computer Vision and Pattern Recognition*, pages 7291–7299, 2017.
- [Chen *et al.*, 2021] Yuxin Chen, Ziqi Zhang, Chunfeng Yuan, Bing Li, Ying Deng, and Weiming Hu. Channel-wise topology refinement graph convolution for skeleton-based action recognition. In *IEEE International Conference on Computer Vision*, pages 13359–13368, 2021.
- [Cheng *et al.*, 2020a] Ke Cheng, Yifan Zhang, Congqi Cao, Lei Shi, Jian Cheng, and Hanqing Lu. Decoupling gcn with dropgraph module for skeleton-based action recognition. In *European Conference on Computer Vision*, pages 536–553, 2020.
- [Cheng *et al.*, 2020b] Ke Cheng, Yifan Zhang, Xiangyu He, Weihan Chen, Jian Cheng, and Hanqing Lu. Skeleton-based action recognition with shift graph convolutional network. In *IEEE Conference on Computer Vision and Pattern Recognition*, pages 183–192, 2020.
- [Cheng *et al.*, 2023] Jiale Cheng, Dongzi Shi, Chenyang Li, Yu Li, Hao Ni, Lianwen Jin, and Xin Zhang. Skeleton-based gesture recognition with learnable paths and signature features. *IEEE Transactions on Multimedia*, 2023.
- [Chéron *et al.*, 2015] Guilhem Chéron, Ivan Laptev, and Cordelia Schmid. P-cnn: Pose-based cnn features for action recognition. In *IEEE International Conference on Computer Vision*, pages 3218–3226, 2015.
- [Chevyrev and Lyons, 2016] Ilya Chevyrev and Terry J Lyons. Characteristic functions of measures on geometric rough paths. *Annals of probability: An official journal of the Institute of Mathematical Statistics*, 44(6):4049–4082, 2016.
- [Driver, 1995] BRUCE K Driver. A primer on riemannian geometry and stochastic analysis on path spaces. 1995.
- [Du *et al.*, 2015] Yong Du, Wei Wang, and Liang Wang. Hierarchical recurrent neural network for skeleton based action recognition. In *IEEE Conference on Computer Vision and Pattern Recognition*, pages 1110–1118, 2015.
- [Escalera *et al.*, 2013] Sergio Escalera, Jordi González, Xavier Baró, Miguel Reyes, Isabelle Guyon, Vassilis Athitsos, Hugo Escalante, Leonid Sigal, Antonis Argyros, Cristian Sminchisescu, et al. Chalearn multi-modal gesture recognition 2013: grand challenge and workshop summary. In *15th ACM on International conference on multimodal interaction*, pages 365–368, 2013.
- [Hambly and Lyons, 2010] Ben Hambly and Terry Lyons. Uniqueness for the signature of a path of bounded variation and the reduced path group. *Annals of Mathematics*, pages 109–167, 2010.
- [He *et al.*, 2016] Kaiming He, Xiangyu Zhang, Shaoqing Ren, and Jian Sun. Deep residual learning for image recognition. In *IEEE Conference on Computer Vision and Pattern Recognition*, pages 770–778, 2016.
- [Hochreiter and Schmidhuber, 1997] Sepp Hochreiter and Jürgen Schmidhuber. Long short-term memory. *Neural Comput.*, 9(8):1735–1780, 1997.
- [Kidger *et al.*, 2020] Patrick Kidger, James Morrill, James Foster, and Terry Lyons. Neural controlled differential equations for irregular time series. *Advances in Neural Information Processing Systems*, 33:6696–6707, 2020.
- [Levin *et al.*, 2013] Daniel Levin, Terry Lyons, and Hao Ni. Learning from the past, predicting the statistics for the future, learning an evolving system. *arXiv preprint arXiv:1309.0260*, 2013.
- [Li *et al.*, 2019a] Chenyang Li, Xin Zhang, Lufan Liao, Lianwen Jin, and Weixin Yang. Skeleton-based gesture recognition using several fully connected layers with path signature features and temporal transformer module. In *AAAI Conference on Artificial Intelligence*, volume 33, pages 8585–8593, 2019.
- [Li *et al.*, 2019b] Maosen Li, Siheng Chen, Xu Chen, Ya Zhang, Yanfeng Wang, and Qi Tian. Actional-structural graph convolutional networks for skeleton-based action recognition. In *IEEE Conference on Computer Vision and Pattern Recognition*, pages 3595–3603, 2019.

- [Liao *et al.*, 2019] Lufan Liao, Xin Zhang, and Chenyang Li. Multi-path convolutional neural network based on rectangular kernel with path signature features for gesture recognition. In *IEEE Visual Communications and Image Processing (VCIP)*, pages 1–4. IEEE, 2019.
- [Liao *et al.*, 2021] Shujian Liao, Terry Lyons, Weixin Yang, Kevin Schlegel, and Hao Ni. Logsig-rnn: a novel network for robust and efficient skeleton-based action recognition. *British Machine Vision Conference*, 2021.
- [Liu *et al.*, 2017a] Jun Liu, Gang Wang, Ping Hu, Ling-Yu Duan, and Alex C Kot. Global context-aware attention lstm networks for 3d action recognition. In *IEEE Conference on Computer Vision and Pattern Recognition*, pages 1647–1656, 2017.
- [Liu *et al.*, 2017b] Mengyuan Liu, Hong Liu, and Chen Chen. Enhanced skeleton visualization for view invariant human action recognition. *Pattern Recognition*, 68:346–362, 2017.
- [Liu *et al.*, 2018] Jun Liu, Amir Shahroudy, Dong Xu, Alex C Kot, and Gang Wang. Skeleton-based action recognition using spatio-temporal lstm network with trust gates. *IEEE Transactions on Pattern Analysis and Machine Intelligence*, 40(12):3007–3021, 2018.
- [Liu *et al.*, 2019a] Bangli Liu, Haibin Cai, Zhaojie Ju, and Honghai Liu. Rgb-d sensing based human action and interaction analysis: A survey. *Pattern Recognition*, 94:1–12, 2019.
- [Liu *et al.*, 2019b] Jun Liu, Amir Shahroudy, Mauricio Perez, Gang Wang, Ling-Yu Duan, and Alex C Kot. Ntu rgb+d 120: A large-scale benchmark for 3d human activity understanding. *IEEE Transactions on Pattern Analysis and Machine Intelligence*, 42(10):2684–2701, 2019.
- [Liu *et al.*, 2020] Ziyu Liu, Hongwen Zhang, Zhenghao Chen, Zhiyong Wang, and Wanli Ouyang. Disentangling and unifying graph convolutions for skeleton-based action recognition. In *IEEE Conference on Computer Vision and Pattern Recognition*, pages 143–152, 2020.
- [Lou *et al.*, 2022] Hang Lou, Siran Li, and Hao Ni. Path development network with finite-dimensional lie group representation. *arXiv preprint arXiv:2204.00740*, 2022.
- [Lyons *et al.*, 2007] Terry J Lyons, Michael Caruana, and Thierry Lévy. *Differential equations driven by rough paths*. Springer, 2007.
- [Lyons *et al.*, 2014] Terry Lyons, Hao Ni, and Harald Oberhauser. A feature set for streams and an application to high-frequency financial tick data. In *2014 International Conference on Big Data Science and Computing*, pages 1–8, 2014.
- [Lyons, 1998] Terry J Lyons. Differential equations driven by rough signals. *Revista Matemática Iberoamericana*, 14(2):215–310, 1998.
- [Lyons, 2014] Terry Lyons. Rough paths, signatures and the modelling of functions on streams. 2014.
- [Ni *et al.*, 2021] Hao Ni, Lukasz Szpruch, Marc Sabate-Vidales, Baoren Xiao, Magnus Wiese, and Shujian Liao. Sig-wasserstein gans for time series generation. In *Second ACM International Conference on AI in Finance*, pages 1–8, 2021.
- [Shahroudy *et al.*, 2016] Amir Shahroudy, Jun Liu, Tian-Tsong Ng, and Gang Wang. Ntu rgb+d: A large scale dataset for 3d human activity analysis. In *IEEE Conference on Computer Vision and Pattern Recognition*, pages 1010–1019, 2016.
- [Shi *et al.*, 2019] Lei Shi, Yifan Zhang, Jian Cheng, and Hanqing Lu. Two-stream adaptive graph convolutional networks for skeleton-based action recognition. In *IEEE Conference on Computer Vision and Pattern Recognition*, pages 12026–12035, 2019.
- [Shi *et al.*, 2020] Lei Shi, Yifan Zhang, Jian Cheng, and Hanqing Lu. Skeleton-based action recognition with multi-stream adaptive graph convolutional networks. *IEEE Transactions on Image Processing*, 29:9532–9545, 2020.
- [Si *et al.*, 2019] Chenyang Si, Wentao Chen, Wei Wang, Liang Wang, and Tieniu Tan. An attention enhanced graph convolutional lstm network for skeleton-based action recognition. In *IEEE International Conference on Computer Vision*, pages 1227–1236, 2019.
- [Song *et al.*, 2020] Yi-Fan Song, Zhang Zhang, Caifeng Shan, and Liang Wang. Stronger, faster and more explainable: A graph convolutional baseline for skeleton-based action recognition. In *28th ACM International Conference on Multimedia*, pages 1625–1633, 2020.
- [Song *et al.*, 2022] Yi-Fan Song, Zhang Zhang, Caifeng Shan, and Liang Wang. Constructing stronger and faster baselines for skeleton-based action recognition. *IEEE Transactions on Pattern Analysis and Machine Intelligence*, 45(2):1474–1488, 2022.
- [Xie *et al.*, 2017] Zecheng Xie, Zenghui Sun, Lianwen Jin, Hao Ni, and Terry Lyons. Learning spatial-semantic context with fully convolutional recurrent network for on-line handwritten chinese text recognition. *IEEE Transactions on Pattern Analysis and Machine Intelligence*, 40(8):1903–1917, 2017.
- [Xu *et al.*, 2022] Kailin Xu, Fanfan Ye, Qiaoyong Zhong, and Di Xie. Topology-aware convolutional neural network for efficient skeleton-based action recognition. In *AAAI Conference on Artificial Intelligence*, volume 36, pages 2866–2874, 2022.
- [Yan *et al.*, 2018] Sijie Yan, Yuanjun Xiong, and Dahua Lin. Spatial temporal graph convolutional networks for skeleton-based action recognition. In *AAAI Conference on Artificial Intelligence*, volume 32, 2018.
- [Yang *et al.*, 2015] Weixin Yang, Lianwen Jin, and Manfei Liu. Chinese character-level writer identification using path signature feature, dropstroke and deep cnn. In *13th International Conference on Document Analysis and Recognition (ICDAR)*, pages 546–550. IEEE, 2015.
- [Yang *et al.*, 2022] Weixin Yang, Terry Lyons, Hao Ni, Cordelia Schmid, and Lianwen Jin. Developing the path

signature methodology and its application to landmark-based human action recognition. In *Stochastic Analysis, Filtering, and Stochastic Optimization: A Commemorative Volume to Honor Mark HA Davis's Contributions*, pages 431–464. Springer, 2022.

[Zhao *et al.*, 2019] Rui Zhao, Kang Wang, Hui Su, and Qiang Ji. Bayesian graph convolution lstm for skeleton based action recognition. In *IEEE International Conference on Computer Vision*, pages 6882–6892, 2019.

[Zhou *et al.*, 2022] Yuxuan Zhou, Zhi-Qi Cheng, Chao Li, Yanwen Fang, Yifeng Geng, Xuansong Xie, and Margret Keuper. Hypergraph transformer for skeleton-based action recognition. *arXiv preprint arXiv:2211.09590*, 2022.

[Zhou *et al.*, 2023] Huanyu Zhou, Qingjie Liu, and Yunhong Wang. Learning discriminative representations for skeleton based action recognition. In *IEEE Conference on Computer Vision and Pattern Recognition*, pages 10608–10617, 2023.

7 Supplementary

7.1 Dual Graph

Previous approaches [Shi *et al.*, 2019; Shi *et al.*, 2020; Chen *et al.*, 2021; Zhou *et al.*, 2023] have commonly adopted a multi-stream architecture, including joint, bone, joint motion and bone motion, with each contributing to improved performance. Inspired by [Li *et al.*, 2019b] that leverages a dual graph as the model input, we also integrate a dual graph to enhance the performance of our model further. The definition of the dual graph is outlined below.

Given a pair of connected joints V_i and joint V_j in the original skeleton graph representation, their bone, denoted by B_{ij} , is defined as follows:

$$B_{ij} = V_i - V_j, \forall i < j, (i, j) \in \mathcal{A}, \quad (6)$$

where \mathcal{A} is the admissible set of the pairs of joints shown in all the nodes of the right graph in Figure 4.

In the dual graph, each bone serves as the vertex of the graph, as depicted in Figure 4. Whether two given bones B_{i_1, j_1} and B_{i_2, j_2} has the edge is determined by whether they have the shared joint, i.e., $1_{i_1=i_2} \cdot 1_{j_1=j_2}$, where 1. is an indicator function. The feature of each node $B_{i,j}$ is given by its vector value of $B_{i,j}$.

This utilization of a dual graph introduces a novel perspective, enhancing the overall performance of our model. It’s clear from Table 1 that incorporating dual graph into the whole model, the overall accuracy can get further improved, especially on the NTU-120 dataset, with 0.4% and 0.5% improvement on X-sub and X-view benchmarks, respectively, indicating the importance of the proposed dual graph.

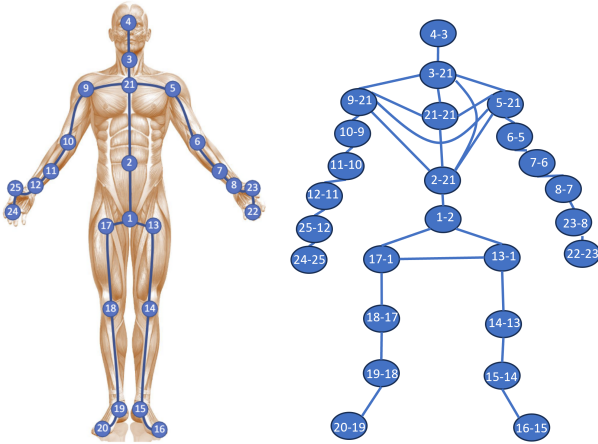


Figure 4: Dual Graph. Left side is the original skeleton representation in NTU dataset. The right side is its dual graph representation. Joint V_{1-2} in the dual graph is the bone B_{12} connecting joint V_1 and V_2 in original graph.

7.2 Detailed Network Architecture

Table 5 gives a detailed network architecture of our proposed approach. The entire network includes 9 blocks, in addition to a global average pooling layer and a linear layer. In

Table 5: Detailed network architecture. P denotes the number of people, L denotes the frame number, M denotes the number of joints, C denotes the feature dimension and N_c denotes the number of classes.

Blocks	Module Type	Output size
Block 1	GCN	$P \times L \times M \times C$
	DevLSTM	$P \times L \times M \times C$
Block 2	GCN	$P \times L \times M \times C$
	DevLSTM	$P \times L \times M \times C$
Block 3	GCN	$P \times L \times M \times C$
	DevLSTM	$P \times L \times M \times C$
Block 4	GCN	$P \times L \times M \times C$
	DevLSTM	$P \times L \times M \times C$
Block 5	GCN	$P \times L \times M \times 2C$
	DevLSTM	$P \times L/2 \times M \times 2C$
Block 6	GCN	$P \times L/2 \times M \times 2C$
	DevLSTM	$P \times L/2 \times M \times 2C$
Block 7	GCN	$P \times L/2 \times M \times 2C$
	DevLSTM	$P \times L/2 \times M \times 2C$
Block 8	GCN	$P \times L/2 \times M \times 4C$
	DevLSTM	$P \times L/4 \times M \times 4C$
Block 9	GCN	$P \times L/4 \times M \times 4C$
	DevLSTM	$P \times L/4 \times M \times 4C$
Global Avg.	-	$1 \times 1 \times 1 \times 4C$
Linear	-	N_c

the table, we report the output size of each block, including GCN and DevLSTM modules, as well as the output size of global average pooling layer and linear layer. In our configuration, the number of people in a video P is set to 2 and 1 on NTU dataset and Chalearn2013 dataset, respectively. The joint number M is 19 on Chalearn2013 dataset and 25 on NTU-60 and NTU-120 datasets. L denotes the frame number. L is 19 on Chalearn2013 dataset, while on NTU60 and NTU120 datasets, we resize all videos with variable lengths to 64 frames. For the base channel size C , we set it as 64. Notably, the temporal dimension is reduced by half at blocks 5 and 8, respectively, by setting the stride = 2 at the DevLSTM module. Last but not least, N_c denotes the number of action classes, which is 120 on the NTU-120 dataset and 20 on the Chalearn2013 dataset, respectively.

7.3 GCN Module

In Figure 5, we present a flow chart illustrating three GCN backbones, serving as the GCN modules employed in this paper for a concise overview. For the details of CTR-GCN and adaptive graph convolution, we refer readers to [Chen *et al.*, 2021] and [Shi *et al.*, 2019], respectively.

The left panel of Figure 5 represents the CTR-GC backbone, while the middle part describes the adaptive graph convolution backbone and the right side is a fixed graph that has no learnable parameters for the adjacency matrix. CTR-GC and adaptive graph convolution share some similarities, as they both utilize three sub-modules and learn the adjacency matrix from the input data. In contrast, CTR-GCN learns

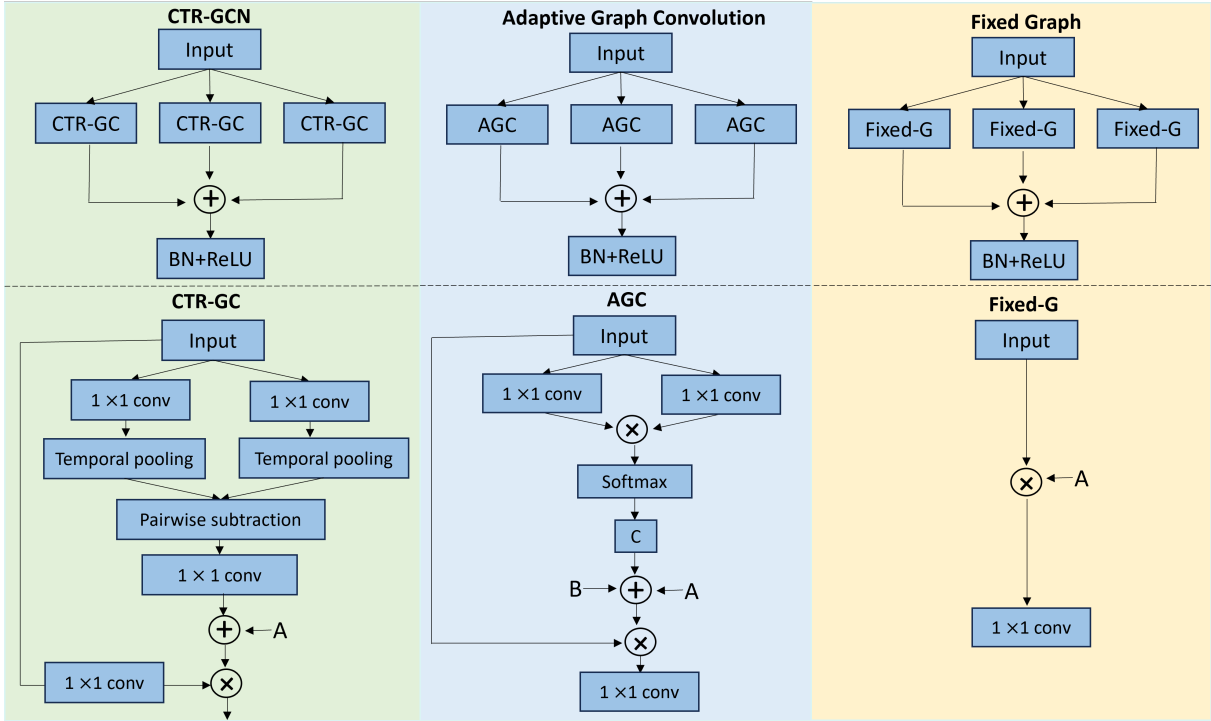


Figure 5: Three GCN Modules used in this paper. The subfigures from left to right represent the CTR-GC module, Adaptive graph convolution module, and the fixed graph, respectively.

the adjacency matrix for each channel, while the channels of adaptive graph convolution share the same adjacency matrix. Besides, adaptive graph convolution utilizes an extra fixed adjacency matrix B representing the physical connection of the body when summing with the learnt adjacency matrix. Different from CTR-GC and adaptive graph convolution, the correlations between joints in the fixed graph are manually defined and remain the same all the time.

7.4 Lie Group & Hidden Size Selection

Table 6: Evaluation of accuracy (%) across different hidden sizes in special Euclidean (SE) and special orthogonal (SO) Lie group on NTU60-Xview benchmark with the joint stream.

Lie Group	Hidden Size				
	8	9	10	11	12
SE	95.6	95.4	95.7	95.5	95.5
SO	95.5	95.5	95.4	95.6	95.4

Given that path development is key to our methodology, the choice of a suitable Lie Group, along with its corresponding hidden size, significantly influences the ultimate performance of the model. Table 6 illustrates that a larger hidden size does not necessarily ensure an enhancement in the model and the best result is obtained by utilizing the special Euclidean group with a hidden size of 10. These important hyperparameters should be tuned based on numerical results in practice.

7.5 Hops-CTRGC

Given three adjacency matrices A_0, A_1, A_2 based on the hops representation, following CTR-GC [Chen *et al.*, 2021], we utilize a network to dynamically learn an adjacency matrix for each channel, adding it with A_k for $k \in \{0, 1, 2\}$. This process can be expressed as:

$$A'_k(X) = A_k + \mathcal{F}_\theta(X) \quad (7)$$

where A'_k represents the updated adjacency matrix, A_k is the initial adjacency matrix for the k -th hop, and $\mathcal{F}_\theta(X) \in \mathbb{R}^{M \times M \times C}$ dynamically captures the spatial correlations of joints from the network, conditioned on the input data $X \in \mathbb{R}^{T \times M \times d}$, considering each channel of the output channels C . Details about the CTR-RC network of $\mathcal{F}_\theta(X)$ can be found in [Chen *et al.*, 2021].

After obtaining the input-conditioned adjacency matrix, the graph convolution is further performed as

$$Z_{t,c} = A'_k(X)_c \cdot (X_t \cdot W_s)_c \quad (8)$$

where $Z \in \mathbb{R}^{T \times M \times C}$ is the output of GCN with the feature dimension C , and $W_s \in \mathbb{R}^{d \times C}$ denotes a feature transformation filter. We sum the outputs from three CTR-GC modules, each employing a distinct adjacency matrix. Subsequently, we apply batch normalization and ReLU activation function to the summation result before sending it to the DevLSTM module.

We compare our proposed 3-hop graph representation with I-In-out representations [Chen *et al.*, 2021] on NTU60

Table 7: Comparison between the graph using I-In-Out and our proposed 3-hop representation in the GCN module on NTU60 dataset.

Graph Representation	X-sub	X-view
3 Hops (J)	90.8	95.7
I-In-Out (J)	90.8	95.5

dataset. As we can see from Table 7, employing the 3-hop graph representation yields better performance compared to I-In-Out representations on X-view benchmark while maintaining equal performance on X-sub benchmark.

7.6 Robustness Analysis

We test the robustness of our approach against the missing frames, missing joints and variable sequence length on NTU60-Xsub benchmark. There are 64 valid frames at the initial stage and We set up two settings for a comprehensive comparison.

In the first experimental setting, we randomly drop or insert a certain number of frames out of the 64 frames. A corresponding drop or insert rate can be obtained by the drop/insert frames divided by 64. In terms of dropping frame, we use linear interpolation based on the remaining frames to fill in the missing frames while for inserting frames, we directly use the linear interpolation to enlarge the original sequence length. We report the accuracy falling number when increasing drop/insert frames at Table 8. As we can see from Table 8, our full model (GCN-DevLSTM) with path development layer always has much less performance degradation compared to CTRGCN [Chen *et al.*, 2021] and our model without path development layer (GCN-LSTM). The accuracy rate of our full model only drops 6.07% at a dropping rate reaching 47% while CTR-GCN falls 18.18% and GCN-LSTM falls 16.56%. Same situation can also be observed when inserting frame.

Table 8: Robustness test on NTU60-Xsub benchmark. This table records the accuracy loss when the number of dropping/inserting frame increases.

Disturbance type	frame number / rate (%)	GCN-DevLSTM	CTRGCN	GCN-LSTM
		Accuracy drop (%)		
Drop	0 / 0	0	0	0
	5 / 8	-0.85	-3.01	-1.39
	10 / 16	-1.35	-5.38	-2.12
	15 / 23	-2.04	-7.01	-3.46
	20 / 31	-2.99	-10.19	-6.23
	30 / 47	-6.07	-18.18	-16.56
	40 / 63	-12.93	-20.65	-20.31
Insert	0 / 0	0	0	0
	6 / 9	-0.82	-1.14	-3.22
	12 / 19	-1.18	-5.09	-1.77
	19 / 30	-1.80	-7.15	-3.13
	25 / 39	-2.76	-8.74	-4.53
	32 / 50	-4.27	-13.73	-9.23
	38 / 59	-5.41	-14.92	-10.88

Due to occlusion, sometimes not all joints can be captured by cameras, leading to some missing values for these occluded joints. To simulate this situation, in the second robustness setting, instead of dropping the whole frame, we randomly drop a certain number of joints in each frame and fill in the values of missing joints in two different ways:

1. Zero filling: fill missing joint values as zeros as it is a standard way to replace NaN values with zero in machine

Table 9: Robustness test on NTU60-Xsub benchmark. This table records the accuracy loss when the number of dropping joint increases and we use zeros and linear interpolation fillings respectively to those missing joints.

Filling way	Drop joint number	GCN-DevLSTM	CTRGCN	GCN-LSTM
		Accuracy drop (%)		
Zeros	0	0	0	0
	1	-7.00	-10.38	-16.58
	2	-13.87	-21.07	-30.50
	3	-19.92	-31.91	-43.50
	4	-27.04	-41.34	-55.50
	5	-34.13	-50.18	-63.96
	6	-41.76	-58.65	-70.16
Linear interpolation	0	0	0	0
	1	-0.09	-0.18	-0.22
	5	-1.24	-1.03	-1.51
	7	-1.96	-1.95	-2.47
	10	-3.65	-3.96	-4.38
	15	-9.77	-11.41	-10.37
	20	-26.74	-31.14	-30.64

learning community.

2. Linear interpolation: Estimate the values at intermediate points based on remaining temporal information of each joint. For time points outside the range, we use zeros.

We show the comparison results of both filling ways at Table 9. As we can see that zero filling is more challenging and the performance of all models degrade fast since it will dramatically destroy the consistency of joints along the temporal dimension. But the advantage to use zero filling is that it does not rely on other frames, making it useful when other frames are unavailable. Regardless of filling ways, our full model with path development layer again achieves the strongest robustness against the missing joints compared to other two models.

Our full model with a path development layer demonstrates powerful robustness against the irregular sampling and variable sequence length, benefiting from its theory foundation.